Varicella-zoster virus infection of human dorsal root ganglia *in vivo*

Leigh Zerboni*†, Chia-Chi Ku*, Carol D. Jones‡, James L. Zehnder‡, and Ann M. Arvin*§

Departments of *Pediatrics, and §Microbiology and Immunology, and ‡Pathology, Stanford University School of Medicine, Stanford, CA 94305

Edited by Bernard Roizman, University of Chicago, Chicago, IL, and approved March 28, 2005 (received for review February 9, 2005)

Varicella-zoster virus (VZV) causes varicella and establishes latency in sensory ganglia. VZV reactivation results in herpes zoster. We developed a model using human dorsal root ganglion (DRG) xenografts in severe combined immunodeficient (SCID) mice to investigate VZV infection of differentiated neurons and satellite cells *in vivo*. DRG engrafted under the kidney capsule and contained neurons and satellite cells within a typical DRG architecture. VZV clinical isolates infected the neurons within DRG. At 14 days postinfection, VZ virions were detected by electron microscopy in neuronal cell nuclei and cytoplasm but not in satellite cells. The VZV genome copy number was 7.1×10^7 to 8.0×10^8 copies per 10^5 cells, and infectious virus was recovered. This initial phase of viral replication was followed within 4–8 weeks by a transition to VZV latency, characterized by the absence of infectious virus release, the cessation of virion assembly, and a reduction in VZV genome copies to 3.7×10^5 to 4.7×10^6 per 10^5 cells. VZV persistence in DRG was achieved without any requirement for VZV-specific adaptive immunity and was associated with continued transcription of the ORF63 regulatory gene. The live attenuated varicella vaccine virus exhibited the same pattern of short-term replication, persistence of viral DNA, and prominent ORF63 transcription as the clinical isolates. VZV-infected T cells transferred virus from the circulation into DRG, suggesting that VZV lymphotropism facilitates its neurotropism. DRG xenografts may be useful for investigating neuropathogenic mechanisms of other human viruses.

herpesvirus | latency | neurotropism | varicella vaccine

Varicella-zoster virus (VZV) is an alphaherpesvirus that causes varicella (chickenpox), establishes latency in sensory ganglia, and may reactivate to cause herpes zoster (1–3). The VZV double-stranded DNA genome encodes at least 70 proteins, expressed as putative immediate-early (IE) regulatory genes, early genes, and late genes. Primary VZV infection is characterized by inoculation of respiratory mucosal epithelium, viral transport to the skin by a cell-associated viremia, cutaneous lesions, and infection of sensory ganglia (1, 2, 4). VZV DNA has been detected in dorsal root ganglia (DRG), trigeminal ganglia, and cranial nerves obtained at autopsy many decades after primary VZV infection (2, 5). VZV reactivation from latency usually causes a localized vesicular rash and pain affecting one cutaneous dermatome, suggesting that VZ virions migrate to the skin along axons from a single ganglion (1). Herpes zoster is medically important because it is often associated with debilitating postherpetic neuralgia, and immunocompromised individuals may develop life-threatening VZV infection (1). Nevertheless, knowledge about the interactions between VZV and the neurons, satellite cells, and fibroblasts that comprise human sensory ganglia is limited to studies of autopsy specimens, and even the cell type that harbors the VZV genome has been controversial (2). Therefore, we have developed a SCID mouse model in which human DRG are established as xenografts to investigate VZV neuropathogenesis *in vivo*.

Like VZV, herpes simplex viruses (HSV) 1 and 2 persist in sensory ganglia (6). Latency-associated transcripts (LATs), which are partly antisense to the regulatory protein ICP0, are expressed in neurons, but HSV proteins are not made. However, VZV has no LAT sequence (2). Transcription, and in some cases, translation, of VZV ORFs for IE genes 4, 62, and 63, as well as early and late genes that encode ribonucleotide reductase (ORF18), nucleocapsid proteins (ORF21 and ORF40), DNA binding protein (ORF29), and viral kinase (ORF66), has been reported in human DRG from autopsies, although observations about specific VZV genes have varied (7–10). Viral glycoprotein expression has not been reported, and our recent investigations in a chimeric nonobese diabetic–SCID mouse–human model suggest that restricted synthesis of the major envelope glycoprotein, gE, blocks the full replicative cycle in human neural cells *in vivo* (11).

Live attenuated varicella vaccines have been introduced for preventing primary VZV infection (12, 13). The vaccine virus was generated by serial passage of a clinical VZV isolate, the parent Oka (pOka) virus, in human and guinea pig embryo fibroblasts. Varicella vaccine virus (vOka) is attenuated and immunogenic in susceptible healthy children. In our SCIDhu model, vOka retained infectivity for human T cells but replicated less effectively in skin when compared with pOka (14). The vOka virus can cause herpes zoster, but whether it is attenuated for neurovirulence is not known (15). We have used the DRG xenograft model to compare the neurotropism of vOka and pOka viruses. In addition, we examined whether VZV-infected T cells could mediate viral transfer into DRG *in vivo*.

Materials and Methods

Animal protocols complied with the Animal Welfare Act and were approved by the Stanford University Administrative Panel on Laboratory Animal Care. Human tissues were provided by Advanced Bioscience Resources (Alameda, CA) and were obtained in accordance with state and federal regulations.

Preparation of DRG Xenografts in SCID Mice. Human fetal DRG were dissected from spinal tissues (gestational age 18–22 weeks) and maintained in supplemented tissue culture media (Mediatech, Washington, DC) before implantation. Six-week-old male C.B-17 *scid/scid* mice (Taconic Farms, Germantown, NY) were sedated, and the left kidney was exposed. A single DRG (1–1.5 mm^3) was inserted under the capsule of the kidney by using a 16-gauge transplant needle; the peritoneal incision was sutured, and skin flaps were stapled. Engraftment was assessed in implants by histology. Serial sections of formalin-fixed paraffin-embedded xenografts (5 μm) were placed on glass slides (four sections per slide), and every 10th slide was stained with hematoxylin/eosin.

This paper was submitted directly (Track II) to the PNAS office.

Abbreviations: DRG, dorsal root ganglia; gB, glycoprotein B; gE, glycoprotein E; HSV, herpes simplex virus; IE, immediate-early; NCAM, neural cell adhesion molecule; pfu, plaque forming units; SCID, severe combined immunodeficient; TEM, transmission electron microscopy; VZV, varicella-zoster virus.

†To whom correspondence should be addressed at: Stanford University School of Medicine, S-356, 300 Pasteur Drive, Stanford, CA 94305. E-mail: zerboni@stanford.edu.

Table 1. VZV primer and probe sequences

Primer name	Sequence
VZV-gB primer (forward)	5′-GATGGTGCATACAGAGAACATTCC-3′
VZV-gB primer (reverse)	5′-CCGTTAAATGAGGCGTGACTAA-3′
VZV-gB probe	5′-(FAM)-TCCGCGCTGCAGGTTCCAGTAAT-(TAMRA)-3′
VZV-ORF62 primer (forward)	5′-TCTTGTCGAGGAGGCTTCTG-3′
VZV-ORF62 primer (reverse)	5′-TGTGTGTCCACCGGATGAT-3′
VZV-ORF62 probe	5′-(FAM)-TCTCGACTGGCTGGGACTTGCG-(TAMRA)-3′
VZV-ORF63 primer (forward)	5′-ATTGAGGCGCCGAATGTTC-3′
VZV-ORF63 primer (reverse)	5′-CTTCACCACCATCATCAGATACG-3′
VZV-ORF63 probe	5′-(FAM)-TTTGCATAGGAGCGCACTGGAATGTG-(TAMRA)-3′

Viruses and Cells. VZV-S and pOka, low-passage clinical isolates, and varicella vaccine virus (Oka-Merck, Merck) were propagated in HELF (human fibroblasts) cells for inoculation of DRG xenografts. Viral titration, done at the time of inoculation, and infectious virus release determinations were done on MeWo cells (melanoma cell line). VZV-infected T cells were propagated by coculture on VZV-infected fibroblasts as described in refs. 4 and 16.

VZV Infection of DRG Xenografts. At 4–12 weeks postimplantation, DRG were infected by direct injection of VZV-infected fibroblasts (≈10 μl, 27-gauge needle). In experiments to investigate the transfer of VZV into DRG by infected T cells, mice were given 3–5 $\times$ 10^6 T cells via tail vein inoculation as described in ref. 4. Mice were killed, and the implanted tissue was recovered at specific times. Tissues were immediately fixed in 4% paraformaldehyde for histological analyses or finely minced in PBS. For infectious virus release assay, one-half of the minced tissue was cocultured with uninfected MeWo cells and passaged six times or until viral plaques were evident. For DNA and RNA extraction, one-half of the minced tissue was treated with either DNAzol or TRIzol (GIBCO), respectively, according to the manufacturer's instructions.

VZV Immunohistochemistry, *in Situ* Hybridization, and Transmission Electron Microscopy (TEM). Detection of VZV and cellular proteins and viral DNA in SCID xenografts was done as described in ref. 14. An antigen retrieval method was used for staining with antibody to NCAM (Chemicon) and synaptophysin (Zymed). Antibodies were used at dilutions recommended by the manufacturer. Rabbit antisera to VZV proteins, IE62 and IE63 (a gift from Paul Kinchington, University of Pittsburgh, Pittsburgh), and rabbit antisera to VZV gE were used at 1:500. Human polyclonal anti-VZV IgG was used at 1:1,000. For immunohistochemistry, slides were developed by using alkaline phosphatase-based enzyme detection methods with 5-bromo-4-chloro-3-indolyl *p*-toluidine salt/nitroblue tetrazolium chloride substrate (Vector Laboratories) or Fast red substrate. FITC- or Texas red-conjugated secondary antibodies were used for immunofluorescence and confocal microscopy (Jackson ImmunoResearch) along with the DAPI nuclear stain. Slides were examined by using a fluorescence (Axiovert 200, Zeiss) or confocal (Axioplan 2 LSM 510, Zeiss) microscope. For TEM, tissue was immersed in 2% glutaraldehyde and processed for embedding. Embedded samples were thin sectioned with a ultramicrotome, placed on copper grids, stained, and viewed with a Philips CM12 transmission electron microscope.

Quantitative PCR and RT-PCR. Quantification of VZV genome copy number and quantitative RT-PCR were accomplished by using the 5′ exonuclease method (17). Briefly, DNA PCR or RNA RT-PCR was performed in the presence of a dual-labeled internally annealing probe (5′ FAM reporter fluorophore and 3′ TAMRA quencher fluorophore). Fluorophore-labeled PCR products were detected in real time by using an Applied Biosystems Prism 7700 instrument. VZV primer sequences and probes were those developed by Pevenstein *et al.* (18) and were synthesized and purified by Operon Technologies (Table 1) (18). Reverse transcription was performed by using the High Capacity cDNA Archive kit (Applied Biosystems). Before reverse transcription, RNA samples were DNase-treated (DNA-free kit, Ambion).

For quantitative PCR to assess genome copy number, each sample was tested for the presence of two viral genes, ORF31 encoding glycoprotein B and ORF62, and for the cellular gene β-actin. To determine VZV transcript copy number, four gene expression targets were measured: VZV-glycoprotein B (gB), VZV-ORF62, VZV-ORF63, and human HPRT (an endogenous control). A separate series of standards for each target and appropriate positive and negative controls were included. β-actin primers and probes were obtained from Applied Biosystems. VZV quantitation standards were prepared and were diluted such that the standard curve spanned 7 logs and was comprised of serial 10-fold dilutions containing 10^6 down to 10^0 targets per well. Quantitative data analysis was performed according to the manufacturer's recommendations to generate amplification plots and standard curves and to determine a quantitative result for each well.

Results

Histological Analysis of DRG Xenografts. By 4 weeks postimplantation, human DRG xenografts appeared as well vascularized tissues (1–2 mm^3) attached to the mouse kidney (Fig. 1*A*). Engraftment was >95% and DRG xenografts survived for at least 8 months. Organotypic features of human DRG before implantation included small and large neuronal cell bodies clustered around sensory nerve fibers encased in a fibroblast-collagen matrix (Fig. 1*B*). Neuronal cell bodies were surrounded by satellite cells and contained a prominent nucleolus within a centrally located nucleus (Fig. 1*B*). DRG xenografts displayed a similar architecture (Fig. 1*C*). Endothelial cells within the microvasculature expressed the human-specific endothelial cell marker PECAM-1 (Fig. 1*D*). Cells in DRG xenografts expressed the human neural-specific markers, neural cell adhesion molecule (NCAM) and synaptophysin. NCAM was distributed extensively on the cell surfaces of neuronal cell bodies and satellite cells (Fig. 1*E*). Synaptophysin, a major synaptic vesicle membrane protein, exhibited its typical diffuse, granular cytoplasmic staining pattern associated with protein accumulation in neurosecretory vesicles (Fig. 1*F*).

VZV Infection of DRG Xenografts. Four weeks postimplantation, DRG xenografts were injected with VZV-S, a clinical isolate [10 μl; 4.5 $\times$ 10^5 plaque forming units (pfu)/ml], or uninfected fibroblasts (10^3 cells). Cytopathic changes were apparent in infected DRG (Fig. 2*B*) compared with mock-infected xeno-

MICROBIOLOGY

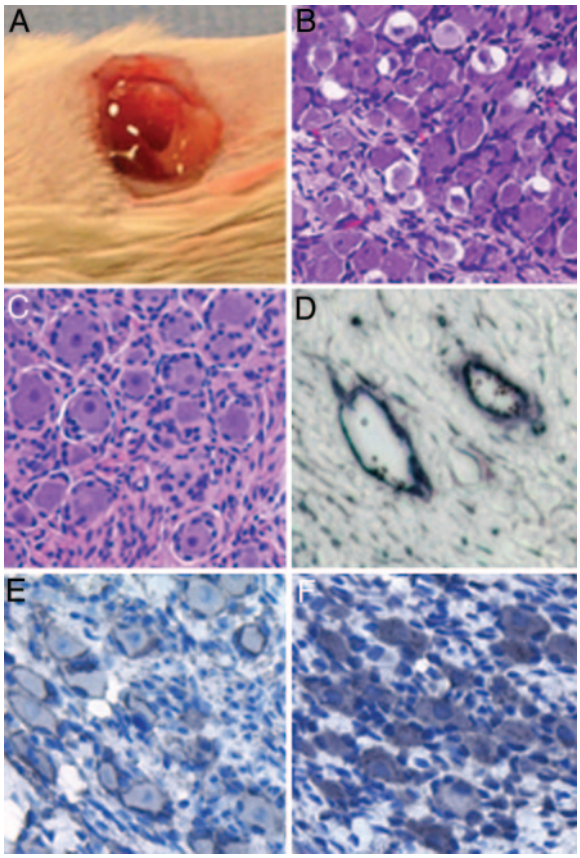

Fig. 1. DRG xenografts in SCID mice. (*A*) Photograph of a DRG xenograft 12 weeks after transplantation (cephalad direction to the left) under the renal capsule. (*B* and *C*) DRG sections before implantation, 18 gestational weeks (*B*) and 32 weeks (*C*) after implantation, stained with hematoxylin/eosin. (*D*) PECAM (anti-CD31)-stained sections from a DRG xenograft, 4 weeks after implantation. (*E*) Neural cell adhesion molecule (NCAM) staining of a section from a DRG xenograft, 4 weeks after implantation. (*F*) Synaptophysin staining of a DRG xenograft section after implantation (4 weeks).

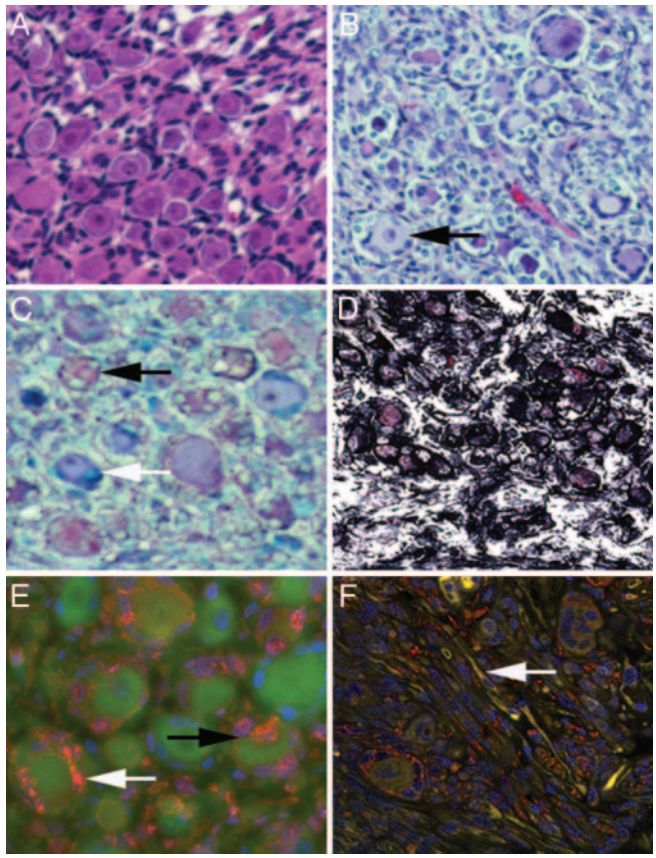

Fig. 2. VZV infection of DRG xenografts. DRG sections were examined 10 days after inoculation with VZV-S or uninfected fibroblasts. (*A* and *B*) hematoxylin/eosin staining of mock-infected (*A*) or VZV-S infected (*B*) xenografts. The black arrow shows a neuronal cell body with contracted cytoplasm and inclusions. (*C*) VZV proteins detected with anti-VZV human polyclonal serum (red), counterstained with methyl green and hematoxylin, showing VZV-positive neurons (black arrow) and VZV-negative neurons (white arrow). (*D*) VZV DNA detected by *in situ* hybridization (red nuclear stain) in DRG sections stained with anti-NCAM antibody (black). (*E*) DRG section stained for Neu-N (green), anti-IE63 antibody (red), and DAPI nuclear stain (blue). IE63 was detected in both neurons (black arrow) and satellite cells (white arrow). (*F*) DRG section stained for gE (red), anti-NCAM (FITC), and DAPI (blue). A fiber is indicated by the white arrowhead.

grafts at 10 days (Fig. 2*A*). Cytoplasmic inclusions (black arrow), denucleated neuronal cell bodies, contracted cytoplasm, and disorganization of surrounding sensory nerve fibers were observed. Many VZV-infected cells were detected by using human polyclonal anti-VZV IgG (Fig. 2*C*, black arrow), but VZV infection did not result in destruction of DRG xenografts. Neurons that did not express VZV proteins were visible even in regions with large numbers of VZV-infected cells (Fig. 2*C*, white arrow). Whereas the hallmark of VZV replication in skin is the formation of polykaryocytes, VZV infection of DRG showed no evidence of cell fusion or syncytia formation (14).

In situ hybridization and immunohistochemistry were used to define the cell types that were susceptible to VZV infection and to distinguish neural cell populations within DRG from fibroblasts that compromise the supportive matrix. Fibroblasts are highly permissive for VZV replication *in vitro*. However, the VZV-specific *in situ* hybridization signal (Fig. 2*D*, red stain) in DRG was primarily in neurons, identified by NCAM expression (Fig. 2*D*, black stain). VZV regulatory proteins, IE62 and IE63, and gE, the predominant glycoprotein, were detected in both neurons and satellite cells by confocal microscopy. IE63 protein was expressed in the nuclei of neurons, identified by neuron-specific antibody Neu-N, and in surrounding satellite cells (Fig. 2*E*). IE62 expression was also localized to nuclei in neurons and satellite cells (data not shown). Glycoprotein E was detected primarily along nerve fibers (Fig. 2*F*, white arrow).

Analysis of VZV-Infected DRG by TEM. Ganglia infected with VZV-S were examined by TEM at 14, 28, and 56 days postinfection and compared with uninfected DRG xenografts (Fig. 3). Virions with characteristics of herpesviral particles were readily identified in neurons at 14 days (6). VZV-infected neurons had fragmented nucleoli, marginated chromatin, and invagination of nuclear membranes (Fig. 3*A*). VZ virions were present in the nuclei and cytoplasm of neurons and in myelinated nerve axons in sensory nerve fascicles (Fig. 3*B Inset*, black arrow) but were not found in satellite cells, including those surrounding extensively infected neurons (Fig. 3 *C* and *D*). Most viral particles lacked an electron-dense core, and none appeared to be fully enveloped. No VZ virions were observed in ganglia harvested 28 or 56 days postinoculation. These DRG exhibited cellular morphology typical of uninfected xenografts.

Viral Replication, Genome Copies, and Viral Gene Transcripts in VZV-Infected DRG. DRG xenografts were inoculated with VZV-S (10 μl; 2.3×10^4 pfu/ml) and harvested 14, 28, and 56 days later. Infectious virus was recovered from five of six ganglia that were tested at 14 days. VZV was not recovered from any of six

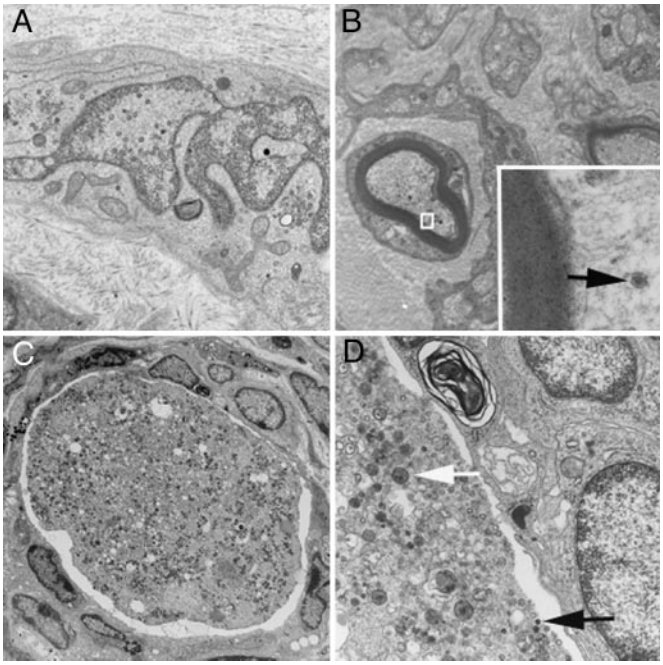

Fig. 3. Analysis of VZV-infected DRG by TEM. DRG sections were examined 14 days after inoculation with VZV-S. (*A*) VZ virions were detected in neuronal cell nuclei and cytoplasm. (Magnification: ×5,000.) (*B*) VZ virions were found in myelinated axons (black arrow). (Magnification: *B*, ×3,800; *B Inset*, ×28,000.) (*C*) Highly infected neuron and surrounding satellite cells. (Magnification: ×1,800.) (*D*) Higher magnification (×10,000). Shown are VZ virions (black arrow) and dense cytoplasmic vesicles consistent with synaptophysin staining by immunohistochemistry (white arrow).

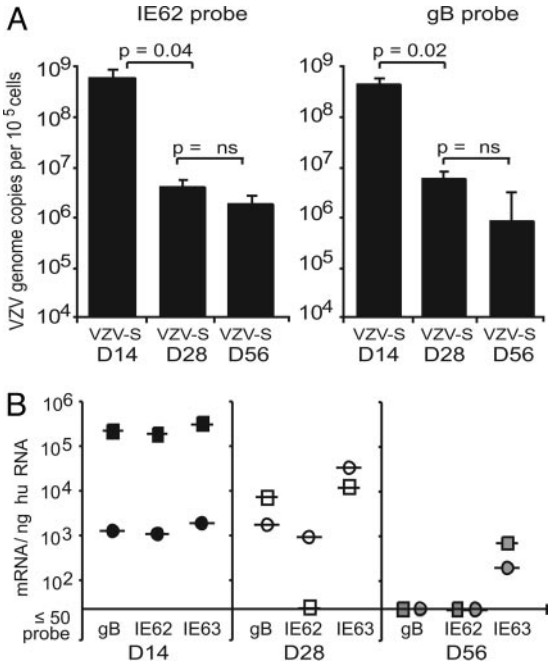

Fig. 4. Assessment of VZV-S-infected DRG xenografts. (*A*) VZV genome copy numbers were detected in VZV-S-infected DRG at day 14, 28, and 56 postinfection. (*Left*) ORF62 copies per 10^5 cells. (*Right*) ORF31 (gB) copies per 10^5 cells. ORF62 copy numbers were adjusted to reflect two copies of ORF62 per VZ genome. The horizontal axis shows days postinfection. (*B*) VZV mRNA transcripts were measured in DRG infected with VZV-S at days 14, 28, and 56 postinfection. Two implants were evaluated at each time point (squares and circles) for mRNA corresponding to gB, IE62, and IE63.

xenografts harvested at day 28 and at day 56, even after six passages of cells inoculated with DRG specimens. Each DRG was tested by quantitative PCR using probes for genes encoding glycoprotein B (ORF31), IE62 (ORF62) and cellular β-actin (Fig. 4*A*). At day 14, VZV genome copy numbers were 7.1×10^7 to 8.0×10^8 copies per 10^5 cells, using the gB probe. By day 28, VZV genome copy numbers dropped significantly to 3.7×10^5 to 9.1×10^6 copies per 10^5 cells, using probes for both gB and IE62 genes ($P = 0.02$ and 0.04, respectively). At day 56, 3.7×10^5 to 4.7×10^6 VZV genome copies per 10^5 cells were detected. These experiments showed that, after an early phase of replication, the VZV genome persisted in human DRG xenografts for at least 8 weeks.

Quantitative RT-PCR was used to detect viral mRNAs corresponding to gB, IE62, and IE63 proteins in DRG inoculated with VZV-S and tested at 14, 28, and 56 days (Fig. 4*B*). VZV gB transcripts were detected in both of two DRG tested at day 14 and at day 28; neither of two DRG had gB transcripts at day 56. IE62 transcripts were present in both of two DRG xenografts tested at day 14, one of two at day 28, and neither of the two at day 56. In contrast, IE63 transcripts were detected at high copy numbers in DRG xenografts tested at days 14, 28, and 56. The presence of mRNA for gB, IE62, and IE63 at the early time point was consistent with recovery of infectious virus from DRG at day 14.

Viral Replication, Genome Copies, and Viral Gene Transcripts in DRG Infected with vOka or pOka Viruses. DRG xenografts were infected with vOka (10 μl; 6.3×10^4 pfu/ml) or pOka (10 μl; 5.3×10^4 pfu/ml) and evaluated 14 and 28 days later. At 14 days, infectious virus was recovered from three of five vOka-infected DRG and four of six pOka-infected DRG. Virus was not recovered from five vOka-infected DRG or four pOka-infected DRG evaluated at 28 days postinfection. VZV genome copy numbers in vOka-infected DRG xenografts were 2.3×10^5 to 2.1×10^7 per 10^5 cells at 14 days compared with 3.9×10^3 to 4.5×10^5 per 10^5 cells at 28 days ($P = 0.03$) (Fig. 5*A*). In pOka-infected DRG, VZV genome copy numbers also declined significantly from 1.5×10^5 to 8.0×10^7 per 10^5 cells at 14 days to 1.5×10^3 to 3.7×10^6 per 10^5 cells at day 28 ($P = 0.04$). VZV genome copy numbers did not differ in vOka- and pOka-infected DRG tested at day 14 or 28. Patterns of replication and genome copy numbers were equivalent in DRG infected with vOka, pOka, and VZV-S.

DRG xenografts were infected with vOka (10 μl; 5.6×10^5 pfu/ml) or pOka (10 μl; 5.0×10^5 pfu/ml) and evaluated by quantitative RT-PCR at 8 weeks (Fig. 5*B*). Transcripts for gB were not detected in any of four implants infected with pOka or any of three implants infected with vOka. ORF62 mRNA was detected in two of four pOka-infected DRG and three of three vOka-infected DRG. ORF63 mRNA was detected in four of four pOka and three of three vOka DRG xenografts. The ORF63 copy number per ng of human RNA was 5-fold higher (938 copies) than ORF62 mRNA (167 copies) in pOka-infected DRG and 3.5-fold higher (7,583 copies) than ORF62 (2,159 copies) in vOka-infected xenografts.

Transfer of VZV to DRG Xenografts by Infected T Cells. SCID mice with DRG xenografts were given VZV-infected tonsil T cells ($3–5 \times 10^6$ cells) by i.v. injection; 16.7% of the T cells expressed VZV proteins by FACS analysis (data not shown). Infectious virus was recovered from one of three DRG harvested 14 days after transfer of VZV-infected T cells. In a second experiment, infectious virus was recovered from one of four DRG tested at 14 days after transfer; VZV DNA was detected in two of these four DRG by PCR and quantitative PCR. VZV genome copy numbers were 9.5×10^6 copies per 10^5 cells and 8.3×10^5 copies

MICROBIOLOGY

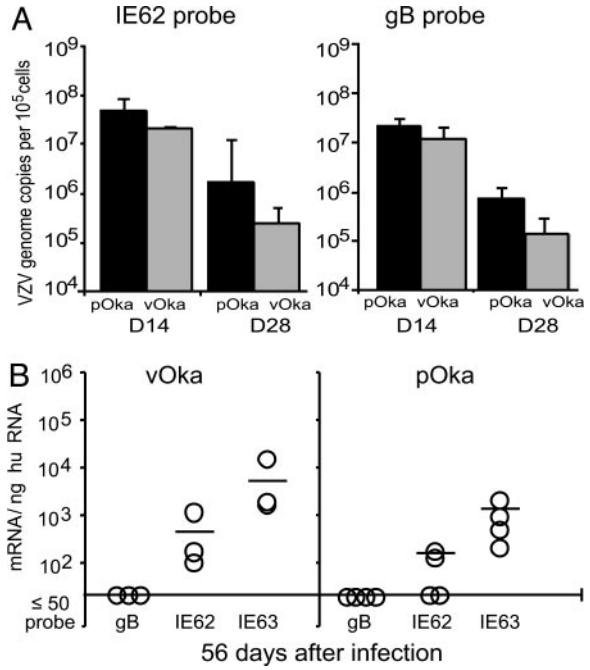

Fig. 5. Assessment of pOka- and vOka-infected DRG xenografts. (*A*) Mean VZV genome copy numbers in DRG infected with pOka (black bars) and vOka (gray bars) using probes for ORF62 (*Left*) and ORF31 encoding gB (*Right*) as viral gene targets. ORF62 copy numbers were adjusted to reflect two copies of ORF62 per VZ genome. (*B*) mRNA transcripts corresponding to gB, IE62, and IE63 were measured in DRG infected with pOka and vOka at 8 weeks postinfection. The horizontal axis shows days postinfection.

per 10^5 cells, respectively, using the gB probe and 3.1×10^6 per 10^5 cells and 2.3×10^5 copies per 10^5 cells, respectively, using the ORF62 probe. These experiments demonstrated that VZV-infected T cells can traffic to, enter, and infect cells within DRG *in vivo*.

Discussion

Because primary VZV and HSV infections are rarely fatal, studying the initial interactions between these human alpha herpesviruses and host cells within human sensory ganglia has not been possible. Investigating VZV infection of human DRG xenografts in this new SCID mouse model has yielded insights about this critical stage in VZV pathogenesis. These experiments demonstrated that VZV infected the neurons within DRG, producing an initial replicative phase that terminated without any host-mediated control by adaptive immune mechanisms. VZV persistence in DRG was associated with continued high levels of ORF63 transcription and suppression of gB gene expression. VZV-infected T cells trafficked to DRG and transferred virus into DRG, suggesting that VZV cell-associated viremia may contribute to VZV neurotropism.

VZV infection of human DRG *in vivo* began with a short period of infectious virus production that did not alter the expression or intracellular distribution of neural cell proteins, such as NCAM and synaptophysin, or the architecture of DRG tissues. VZ virions were abundant in nuclei and cytoplasm of neurons but were not detected in adjacent satellite cells, indicating that neurons were the permissive cell type within DRG. Detection of VZ particles in myelinated nerve fibers suggested the potential for axonal transport and paralleled observations about HSV and pseudorabies virus (PRV) (6, 19). Virion envelopment was restricted in neurons, in contrast to the formation of fully enveloped virions in VZV-infected skin xenografts (20). The intracellular localization of IE62 and IE63 proteins, which are components of the virion tegument as well as regulators of viral gene transcription, was predominantly nuclear, whereas the major VZV envelope glycoprotein, gE, was detected primarily along nerve fibers. The altered distribution of key viral proteins may explain the incomplete virion assembly in infected neurons (21–24). Cytopathic changes were limited to individually infected neurons, with no evidence of syncytia formation. Thus, VZV-infected neurons exhibited an intrinsic resistance to VZV-induced cell fusion that dominates the pathogenesis of VZV skin infection (20). Virions were not detected in satellite cells, whereas some autopsy studies have suggested that these cells may be a reservoir for VZV (25, 26). The presence of IE62 and IE63 proteins in nuclei of satellite cells during the replicative phase of VZV infection of DRG xenografts indicates that VZV may cause an abortive infection in nonneuronal cells.

The limited cytopathic changes associated with acute VZV infection of DRG xenografts suggest that an intrinsic viral mechanism represses viral gene transcription and supports the transition to latency in differentiated neurons *in vivo*. Local cellular control mechanisms, such as the production of IFN-α, that we observed in skin may also contribute to this process (1, 4). By 4 weeks, infectious virus was not recovered from DRG xenografts, and by 8 weeks, virion assembly had stopped and the late envelope glycoprotein, gB, was no longer transcribed. VZV genome copy numbers declined by 2–3 logs between 14 days and 28–56 days after DRG infection, to a range of 10^5 to 10^6 copies per 10^5 cells. When the VZV DNA burden has been evaluated in autopsied human ganglia, estimates have differed depending on the PCR method used and whether VZV DNA was assumed to persist in satellite cells (26–30). Pevenstein *et al.* (18) reported a mean of 258 copies per 10^5 cells, whereas Cohrs *et al.* (29) reported a range of 577–55,543 copies per 10^5 cells. These autopsy studies did not document the years since primary VZV infection, but the usual interval is likely to have been at least two decades. By 8 weeks, VZV genome copy numbers in DRG xenografts were in the upper range of the VZV DNA burden measured in autopsied DRG, indicating that control of infection is achieved rapidly. Whereas VZV-specific T cells are required to limit VZV reactivations that result in herpes zoster, these experiments provide the first evidence that adaptive immunity is not required for establishing VZV persistence in human neurons *in vivo*.

DRG xenograft experiments permitted sequential assessments showing that VZV infection of neurons was characterized by an early transition to cessation of virion assembly and transcriptional repression of the late gene encoding gB. ORF62 transcription persisted in some DRG, but ORF63 mRNA was detected consistently and remained at levels that were 3.5- to 5-fold higher than ORF62. Transcription of several VZV genes has been described in autopsy specimens, including ORFs 21, 29, 62, and 63, in particular (7, 31). Detection of IE62, IE63, and other viral regulatory proteins, ORFs 4, 21, 29, and 66, has also been reported (9, 10). However, expression of these VZV genes in autopsy specimens might be triggered by host demise or occur during the interval required to obtain ganglion tissue. Investigations of HSV-1 latency in mice have documented altered patterns of host cell protein expression that may affect virus–host cell interactions in ganglia removed at different intervals and held as explants (32). In contrast, DRG xenograft experiments allowed immediate preservation of VZV-infected ganglia. VZV mRNAs corresponding to ORFs 4, 21, 29, 62, and 63 have been detected in both neurons and satellite cells in rodent models (33–35), but events in human DRG neuropathogenesis may not be fully captured in these models because VZV is highly species-specific and does not replicate in rodent sensory ganglia. Thus, observations using DRG xenografts provide an important validation of the evidence that ORF63 transcription is a prominent characteristic of VZV latency, as described in autopsy and

rodent model studies (7, 9, 11, 36). One hypothesis is that latency is mediated by the functions of IE63 that down-regulate VZV gene transcription, as opposed to those that enhance IE62-mediated transactivation of some viral genes (37–39). It will be of interest to examine the contributions of other VZV ORFs reported to be expressed in autopsied ganglia and to test VZV mutants in the SCIDhu DRG model.

By analogy with HSV, VZV is presumed to gain access to sensory ganglia by retrograde transport from sites of replication in skin, and VZV proteins have been identified in nerve fibers within VZV skin lesions (40). However, VZV has been detected in sensory ganglia from immunocompromised children with primary VZV infection who died before skin lesions appeared, suggesting that VZV may also be delivered to DRG during cell-associated viremia (1). We have reported that VZV-infected T cells transferred the virus to skin xenografts in SCIDhu mice, resulting in characteristic cutaneous lesions (4). These experiments in the DRG model indicate that VZV-infected T cells might also contribute to the delivery of VZV to neurons, as a second mechanism for VZV entry into neurons and the establishment of latency in sensory ganglia.

The live attenuated varicella vaccine virus exhibited the same pattern of short-term replication, persistence of viral DNA, and prominent ORF63 transcription in DRG as the clinical isolates, pOka and VZV-S. Infection of skin xenografts with vOka was associated with slower progression of cutaneous lesions, decreased viral protein synthesis, and lower yields of infectious virus, as compared with pOka or VZV-S (14, 41). We have proposed that the clinical attenuation of vOka vaccine results from this reduced capacity to replicate in skin, allowing a longer interval for inducing adaptive antiviral immune responses (42). Our DRG experiments suggest that vOka attenuation by serial passage in cultured cells has not altered infectivity for neurons or the capacity to establish a transcriptionally repressed latent state. However, the clinical experience in immunocompromised children indicates that vOka reactivates less often than wild-type VZV (13). Therefore, our observations suggest that herpes zoster may be less common after vaccination because initial access of vOka to neural cells is reduced by limited skin replication and little or no cell-associated viremia, rather than altered neurovirulence.

DRG xenografts in SCID mice should be useful for defining molecular mechanisms of VZV neuropathogenesis through studies of VZV mutants, analyzing the innate neuronal cell responses that control VZV replication, and evaluating potential "second generation" varicella vaccines to eliminate vaccine virus latency. DRG xenografts may be useful in exploring the differences between VZV and HSV that suggest a more stable repression of VZV in DRG, including the failure to recover infectious VZV from explanted human ganglia and the much lower frequency of clinical episodes of VZV reactivation. DRG xenografts in SCID mice may have general value for investigating the neurotropism of other human viral pathogens.

We thank Nafisa Ghori for assistance with electron microscopy and Jeremy Jones, a graduate student in the A.M.A. laboratory, for his technical assistance. This work was supported by National Institute of Allergy and Infectious Diseases Grants AI20459 and AI053846.

1. Arvin, A. M. (2001) in *Fields Virology*, eds. Knipe, D. M. & Howley, P. M. (Lippincott Williams & Wilkins, Philadelphia), Vol. 2, pp. 2731–2767.
2. Cohen, J. I. & Straus, S. E. (2001) in *Fields Virology*, eds. Knipe, D. M. & Howley, P. M. (Lippincott Williams & Wilkins, Philadelphia), Vol. 2, pp. 2707–2730.
3. Gilden, D. H., Kleinschmidt-DeMasters, B. K., LaGuardia, J. J., Mahalingam, R. & Cohrs, R. J. (2000) *N. Engl. J. Med.* **342,** 635–645.
4. Ku, C. C., Zerboni, L., Ito, H., Graham, B. S., Wallace, M. & Arvin, A. M. (2004) *J. Exp. Med.* **200,** 917–925.
5. Gilden, D. H., Vafai, A., Shtram, Y., Becker, Y., Devlin, M. & Wellish, M. (1983) *Nature* **306,** 478–480.
6. Roizman, B. & Knipe, D. M. (2001) in *Fields Virology*, eds. Knipe, D. M. & Howley, P. M. (Lippincott Williams & Wilkins, Philadelphia), Vol. 2, pp. 2399–2459.
7. Mahalingam, R., Wellish, M., Cohrs, R., Debrus, S., Piette, J., Rentier, B. & Gilden, D. H. (1996) *Proc. Natl. Acad. Sci. USA* **93,** 2122–2124.
8. Kennedy, P. G., Grinfeld, E. & Bell, J. E. (2000) *J. Virol.* **74,** 11893–11898.
9. Lungu, O., Panagiotidis, C. A., Annunziato, P. W., Gershon, A. A. & Silverstein, S. J. (1998) *Proc. Natl. Acad. Sci. USA* **95,** 7080–7085.
10. Cohrs, R. J., Gilden, D. H., Kinchington, P. R., Grinfeld, E. & Kennedy, P. G. (2003) *J. Virol.* **77,** 6660–6665.
11. Baiker, A., Fabel, K., Cozzio, A., Zerboni, L., Sommer, M., Uchida, N., He, D., Weissman, I. & Arvin, A. M. (2004) *Proc. Natl. Acad. Sci. USA* **101,** 10792–10797.
12. Takehashi, M., Otsuka, T., Okuno, Y., Asano, Y., Yazaki, T. & Isomura, S. (1974) *Lancet* **2,** 1288–1290.
13. Gershon, A. A., Takehashi, M. & Seward, J. (2002) in *Vaccines*, eds. Plotkin, S. & Orenstein, W. (Saunders, Philadelphia), pp. 783–824.
14. Moffat, J. F., Zerboni, L., Kinchington, P. R., Grose, C., Kaneshima, H. & Arvin, A. M. (1998) *J. Virol.* **72,** 965–974.
15. Hardy, I., Gershon, A. A., Steinberg, S. P. & LaRussa, P. (1991) *N. Engl. J. Med.* **325,** 1545–1550.
16. Zerboni, L., Sommer, M., Ware, C. F. & Arvin, A. M. (2000) *Virology* **270,** 278–285.
17. Holland, P. M., Abramson, R. D., Watson, R. & Gelfand, D. H. (1991) *Proc. Natl. Acad. Sci. USA* **88,** 7276–7280.
18. Pevenstein, S. R., Williams, R. K., McChesney, D., Mont, E. K., Smialek, J. E. & Straus, S. E. (1999) *J. Virol.* **73,** 10514–10518.
19. Smith, G. A., Gross, S. P. & Enquist, L. W. (2001) *Proc. Natl. Acad. Sci. USA* **98,** 3466–3470.
20. Besser, J., Ikoma, M., Fabel, K., Sommer, M. H., Zerboni, L., Grose, C. & Arvin, A. M. (2004) *J. Virol.* **78,** 13293–13305.
21. Stevenson, D., Xue, M., Hay, J. & Ruyechan, W. T. (1996) *J. Virol.* **70,** 658–662.
22. Bontems, S., Di Valentin, E., Baudoux, L., Rentier, B., Sadzot-Delvaux, C. & Piette, J. (2002) *J. Biol. Chem.* **277,** 21050–21060.
23. Baiker, A., Bagowski, C., Ito, H., Sommer, M., Zerboni, L., Fabel, K., Hay, J., Ruyechan, W. & Arvin, A. M. (2004) *J. Virol.* **78,** 1181–1194.
24. Lynch, J. M., Kenyon, T. K., Grose, C., Hay, J. & Ruyechan, W. T. (2002) *Virology* **302,** 71–82.
25. Croen, K. D., Ostrove, J. M., Dragovic, L. J. & Straus, S. E. (1988) *Proc. Natl. Acad. Sci. USA* **85,** 9773–9777.
26. Lungu, O., Annunziato, P. W., Gershon, A., Staugaitis, S. M., Josefson, D., LaRussa, P. & Silverstein, S. J. (1995) *Proc. Natl. Acad. Sci. USA* **92,** 10980–10984.
27. Mahalingam, R., Wellish, M., Lederer, D., Forghani, B., Cohrs, R. & Gilden, D. (1993) *J. Virol.* **67,** 2381–2384.
28. LaGuardia, J. J., Cohrs, R. J. & Gilden, D. H. (1999) *J. Virol.* **73,** 8571–8577.
29. Cohrs, R. J., Randall, J., Smith, J., Gilden, D. H., Dabrowski, C., van Der Keyl, H. & Tal-Singer, R. (2000) *J. Virol.* **74,** 11464–11471.
30. Levin, M. J., Cai, G. Y., Manchak, M. D. & Pizer, L. I. (2003) *J. Virol.* **77,** 6979–6987.
31. Cohrs, R. J., Barbour, M. & Gilden, D. H. (1996) *J. Virol.* **70,** 2789–2796.
32. Sawtell, N. M. & Thompson, R. L. (2004) *J. Virol.* **78,** 7784–7794.
33. Sadzot-Delvaux, C., Merville-Louis, M. P., Delree, P., Marc, P., Piette, J., Moonen, G. & Rentier, B. (1990) *J. Neurosci. Res.* **26,** 83–89.
34. Kennedy, P. G., Grinfeld, E., Bontems, S. & Sadzot-Delvaux, C. (2001) *Virology* **289,** 218–223.
35. Sato, H., Pesnicak, L. & Cohen, J. I. (2002) *J. Virol.* **76,** 3575–3578.
36. Cohen, J. I., Cox, E., Pesnicak, L., Srinivas, S. & Krogmann, T. (2004) *J. Virol.* **78,** 11833–11840.
37. Jackers, P., Defechereux, P., Baudoux, L., Lambert, C., Massaer, M., Merville-Louis, M. P., Rentier, B. & Piette, J. (1992) *J. Virol.* **66,** 3899–3903.
38. Kost, R. G., Kupinsky, H. & Straus, S. E. (1995) *Virology* **209,** 218–224.
39. Spengler, M., Niesen, N., Grose, C., Ruyechan, W. T. & Hay, J. (2001) *Arch. Virol. Suppl.*, 71–79.
40. Annunziato, P., Lungo, O., Panagiotidis, C., Zhang, J., Silvers, D., Gershon, A. & Silverstein, S. (2000) *J. Virol.* **74,** 2005–2010.
41. Zerboni, L., Hinchliffe, S., Sommer, M. H., Ito, H., Besser, J., Stamatis, S., Cheng, J., Distefano, D., Kraiouchkine, N., Shaw, A. & Arvin, A. M. (2005) *Virology* **332,** 337–346.
42. Arvin, A. M. (2001) *Virology* **284,** 153–158.